

Prediction of Nonlinear Specific Heat During Single Crystal HMX Phase Transition

C. W. Williams and K. Matouš*

*Department of Aerospace and Mechanical Engineering,
University of Notre Dame, Notre Dame, Indiana, 46556*

(Dated: January 13, 2023)

We develop a thermodynamically consistent chemo-thermo-mechanical model for the $\beta \rightarrow \delta$ phase transition of energetic HMX crystals. In contrast to previous models, which either considered specific heat to be a constant or utilized a calibrated function, this model provides novel expressions for the specific heats at constant volume and constant elastic strains derived directly from continuum mechanics. In addition, the model provides a novel prediction for the critical temperature at which the chemical heating rate achieves its extremum for Arrhenius kinetics. The numerical solution predicts highly nonlinear specific heat behavior including order of magnitude changes.

Phase transition is a chemo-thermo-mechanical (CTM) process that is common in nature [1–4], occurs in systems which are not in thermodynamic equilibrium, and is associated with exotic material behavior.

One such exotic behavior pertains to negative specific heats known to astronomers and Lynden-Bell and Lynden-Bell [5] related this exotic behavior to the large variations associated with phase transitions.

In addition to negative values in astrophysics, experiments have also shown large changes in specific heat values for typical engineering materials. Differential scanning calorimetry (DSC) measurements of several phase change materials have shown order of magnitude variations (i.e., between $\mathcal{O}(10^3)$ and $\mathcal{O}(10^4)$ [J/(kg·K)]) [1, 6, 7]. Moreover, phase transitions in minerals have given rise to very large nonlinear variations in their volume and density as well as softening of the bulk modulus and other elastic constants [8]. This softening response of the bulk modulus has also been experimentally observed during the phase transition in NIPA gels [9]. It has long been recognized that conventional phase transition models cannot successfully describe the pressure and temperature (P-T) space, and that novel theories are required [10, 11].

In this work, we develop a novel thermodynamically consistent model to describe the continuum level chemistry, thermodynamics, and mechanics of materials. The model describes phase transition and makes predictions on the exotic behavior of the specific heats. The model also highlights the importance of the coefficient of thermal expansion (CTE) and bulk modulus. The model is nonlinear, calibrated using experimental data, and includes strong coupling between all relevant fields. We also derive a novel prediction for the critical temperature at which the chemical heating rate achieves its extremum for Arrhenius kinetics.

We posit the plausibility of exotic specific heat behavior in phase transitioning systems beyond those aforementioned since similar nonlinear, non-equilibrium processes have often been observed [12–14]. In particular, we select octahydro-1,3,5,7-tetranitro-1,3,5,7-tetrazocine (HMX), which is an important compound for solid rocket

propellants. HMX transitions between four solid phase polymorphs [15]. Phase change between the unstable β -HMX and δ -HMX polymorphs is coupled with a 6.7% increase in volume [16]. An experimental effort has been directed towards understanding the chemical [17–20] and thermo-mechanical [16] behavior of HMX. A substantial amount of work has also been done on the modeling and simulation of HMX [20].

We derive our model in the context of a multiplicative decomposition of the total deformation gradient, \mathbf{F} , into thermal (\mathbf{F}_θ) and elastic (\mathbf{F}_e) parts given by [21]

$$\mathbf{F}({}^0\vec{x}, t) \equiv {}^0\nabla\phi({}^0\vec{x}, t) = \mathbf{F}_e \mathbf{F}_\theta, \quad (1)$$

where $\vec{x} = \phi({}^0\vec{x}, t) : \Omega_0 \rightarrow \Omega$ is the motion of the body from its reference to its current configuration. Here, ${}^0\vec{x}$ and \vec{x} are the material and spatial coordinates of the body, respectively. We utilize an isotropic thermal deformation gradient,

$$\mathbf{F}_\theta = \vartheta(\theta)\mathbf{1}, \quad \vartheta(\theta) = \exp\left[\int_{\theta_0}^{\theta} \alpha(\tilde{\theta}) d\tilde{\theta}\right], \quad (2)$$

where $\vartheta(\theta)$ represents the thermal stretch ratio, $\alpha(\theta)$ is the CTE, and $\mathbf{1}$ is the second order identity tensor. For constant CTE, $\vartheta = \exp[\alpha(\theta - \theta_0)] \approx 1 + \alpha(\theta - \theta_0)$ in the limit of small temperature change. It is convenient to define the elastic left Cauchy-Green tensor $\mathbf{b}_e \equiv \mathbf{F}_e \mathbf{F}_e^\top$ which, for isotropic thermal deformation, can be expressed as $\mathbf{b}_e = \vartheta^{-2}\mathbf{b}$ where $\mathbf{b} = \mathbf{F} \mathbf{F}^\top$ is the left Cauchy-Green tensor.

From here, we present the governing equations of the CTM model. The conservation of mass reads

$$\rho_0 = J\rho, \quad (3)$$

where $\rho_0({}^0\vec{x})$ and $\rho(\vec{x}, t)$ are the densities in the reference and current configurations, respectively, and $J({}^0\vec{x}, t) = \det(\mathbf{F})$. From the conservation of energy, we derive

$$\rho c_p \dot{\theta} + \nabla \cdot \vec{\mathbf{q}} = \rho(r + q_c + q_e), \quad (4)$$

where c_p is the specific heat at constant elastic strains, r is the energy source per unit mass, and q_c and q_e are the chemical and elastic heating terms per unit mass, re-

spectively. Here, $(\dot{\bullet})$ indicates the material time derivative. We assume Fourier's model of heat conduction, $\vec{\mathbf{q}} = -\mathbf{\Lambda} \nabla \theta = -\mathbf{\Lambda} \mathbf{1} \nabla \theta$, where $\mathbf{\Lambda}$ is the isotropic thermal conductivity. The conservation of chemical species for the $\beta \rightarrow \delta$ reaction takes the form

$$\rho \dot{y}_\gamma = M_\gamma \nu_\gamma r_c, \quad (5)$$

where y_γ , M_γ , and ν_γ are the mass fraction, molar mass, and stoichiometric coefficient of the γ -th chemical species, respectively, and r_c is the rate of reaction [22]. We neglect mass diffusion, since the length scales involved are much larger than the atomic scale, and consider $M_\beta = M_\delta$. Finally, the conservation of linear momentum is

$$\nabla \cdot \boldsymbol{\sigma} + \rho \vec{\mathbf{f}} = \vec{\mathbf{0}}, \quad (6)$$

where $\boldsymbol{\sigma} = \boldsymbol{\sigma}^\top$ is the Cauchy stress and $\vec{\mathbf{f}}$ is the body force per unit mass. Quasi-static motion is assumed since the time scales for the problem at hand are much slower than the time scales associated with mechanical waves. All governing equations are solved with respect to the relevant initial and boundary conditions.

To close the system, the Helmholtz free energy reads

$$\varphi(\theta, y_\gamma, \mathbf{b}_e) = \varphi_c(\theta, y_\gamma) + \varphi_\theta(\theta) + \varphi_e(\mathbf{b}_e, \theta), \quad (7)$$

where φ_c , φ_θ , and φ_e , are the chemical, thermal, and elastic parts per unit mass, respectively [23]. We take φ_c to be

$$\varphi_c(\theta, y_\gamma) = \sum_{\gamma=1}^{N_s} \frac{\chi_\gamma}{M_\gamma} y_\gamma, \quad (8)$$

where χ_γ is the chemical potential per mole of species γ which is assumed to be, at most, a linear function of temperature. The rate of reaction, r_c , is defined using the law of mass action as [22]

$$r_c = k_c \prod_{\gamma=1}^{N_s} \left(\frac{\rho y_\gamma}{M_\gamma} \right)^{\nu'_\gamma}, \quad k_c = A \hat{A}(\dot{\theta}) \exp\left(-\frac{E_a}{R_u \theta}\right), \quad (9)$$

where we neglect the reverse reaction. Here, ν'_γ is the forward stoichiometric coefficient for the γ -th species. We model the reaction constant, k_c , using a modified Arrhenius law where A , E_a , and R_u are the pre-exponential factor, activation energy, and universal gas constant. \hat{A} is a temperature rate dependent correction factor [20].

Inspired by linear theory, which gives the canonical relation between heat capacities $-\theta(\partial^2 \varphi_\theta / \partial \theta^2) = {}^0 c_p = {}^0 c_v + 9\alpha_0^2 \theta_0 \kappa_0 / \rho_0$ [23], we take

$$\varphi_\theta(\theta) = - \int_{\theta_0}^{\theta} \int_{\theta_0}^{\hat{\theta}} \left(\frac{{}^0 c_v}{\hat{\theta}} + \frac{9\alpha^2(\hat{\theta}) \kappa(\hat{\theta})}{\rho_0} \right) d\hat{\theta} d\tilde{\theta}, \quad (10)$$

where ${}^0 c_v$ is the initial specific heat capacity at constant volume and $\kappa(\theta)$ is temperature dependent bulk modulus.

Finally, we take φ_e to follow the volumetric deviatoric

split relation given by [24, 25]

$$\rho_0 \varphi_e(\mathbf{b}_e, \theta) = J_\theta (\widehat{W}_e + U_e) = J_\theta W_e, \quad (11a)$$

$$\widehat{W}_e(\mathbf{b}_e, \theta) = \frac{1}{2} \mu(\theta) [J_e^{-2/3} \text{tr}(\mathbf{b}_e) - 3], \quad (11b)$$

$$U_e(J_e, \theta) = \frac{1}{4} \kappa(\theta) [(J_e - 1)^2 + (\ln J_e)^2], \quad (11c)$$

where $J_e = \det(\mathbf{F}_e)$ and $J_\theta = \det(\mathbf{F}_\theta)$. Note the functional dependency of J_e on \mathbf{b}_e , namely $J_e^2 = \det(\mathbf{b}_e)$. Here, $\mu(\theta)$ is the temperature dependent shear modulus.

Next, we consider the Clausius-Duhem inequality [26],

$$\boldsymbol{\sigma} : \mathbf{1} - \rho \dot{\varphi} - \rho \dot{\theta} \eta - \frac{1}{\theta} \vec{\mathbf{q}} \cdot \nabla \theta \geq 0, \quad (12)$$

where $\mathbf{1} = \dot{\mathbf{F}} \mathbf{F}^{-1}$ is the total velocity gradient. Through the Coleman-Nole procedure [27], we attain the Cauchy stress as

$$\boldsymbol{\sigma} = 2\rho \frac{\partial \varphi}{\partial \mathbf{b}_e} \mathbf{b}_e = \frac{2}{J_e} \frac{\partial W_e}{\partial \mathbf{b}_e} \mathbf{b}_e, \quad (13)$$

with pressure, $p \equiv \partial U_e / \partial J_e$. We also obtain the entropy as

$$\eta \equiv - \frac{\partial \varphi}{\partial \theta} \Big|_{\mathbf{F}} = \frac{\alpha \boldsymbol{\sigma} : \mathbf{1} J}{\rho_0} - \frac{\partial \varphi}{\partial \theta} \Big|_{\mathbf{b}_e}. \quad (14)$$

In this work, $\partial y / \partial x|_z$ denotes the derivative of quantity y with respect to x at fixed z . Furthermore, we ascertain the chemical and thermal dissipation inequalities as

$$\mathcal{D}_c \equiv - \sum_{\gamma=1}^{N_s} \frac{\partial \varphi}{\partial y_\gamma} \dot{y}_\gamma \geq 0, \quad (15a)$$

$$\mathcal{D}_\theta \equiv - \frac{1}{\theta} \vec{\mathbf{q}} \cdot \nabla \theta \geq 0. \quad (15b)$$

We deduce

$$c_p \equiv \theta \frac{\partial \eta}{\partial \theta} \Big|_{\mathbf{b}_e} = {}^0 c_v + \frac{9\alpha^2 \theta}{\rho_0} (\kappa + pJ) + \frac{3pJ}{\rho_0} \frac{d\alpha}{d\theta} \theta - \alpha \boldsymbol{\ell}_e : \mathbf{1} - \theta \frac{\partial^2 \varphi_e}{\partial \theta^2} \Big|_{\mathbf{b}_e} \quad (16)$$

as the specific heat at constant elastic strains. Here, $\boldsymbol{\ell}_e = -\theta(\partial \boldsymbol{\sigma} / \partial \theta)|_{\mathbf{b}_e} / \rho$ is the spatial latent heat tensor at constant elastic strains. We note that for temperature independent κ and μ the specific heat at constant elastic strains, c_p , reduces to a classical specific heat at constant pressure. The chemical and elastic heating terms are

$$q_c \equiv - \sum_{\gamma=1}^{N_s} \frac{\partial e}{\partial y_\gamma} \dot{y}_\gamma = -k_c (1 - y_\delta) \Delta e^{\text{rxn}}, \quad (17a)$$

$$q_e \equiv - \left[2\theta \frac{\partial \eta}{\partial \mathbf{b}_e} \mathbf{b}_e \right] : \mathbf{1}_e, \quad (17b)$$

where $e = \varphi + \theta \eta$ is the internal energy per unit mass, $\Delta e^{\text{rxn}} = \Delta h^{\text{rxn}} - \Delta(3p/\rho)$ is the change in the internal energy, Δh^{rxn} is the heat of reaction per unit mass and

$\mathbf{l}_e = \dot{\mathbf{F}}_e \mathbf{F}_e^{-1}$ is the elastic velocity gradient. The specific heat at constant total deformation (i.e., constant volume) reads

$$\begin{aligned} c_v &\equiv \theta \frac{\partial \eta}{\partial \theta} \Big|_{\mathbf{F}} = -\theta \frac{\partial^2 \varphi}{\partial \theta^2} \Big|_{\mathbf{F}} = c_p - \alpha \ell : \mathbf{1} \quad (18) \\ &= c_p - \frac{9\alpha^2 \theta}{\rho} \left[J_e \frac{\partial^2 U_e}{\partial J_e^2} \right] + \frac{3\alpha \theta}{\rho} \frac{\kappa'}{\kappa} p, \end{aligned}$$

where $\ell \equiv -\theta(\partial \sigma / \partial \theta)_{\mathbf{F}} / \rho$ is the spatial latent heat tensor and $\kappa' = d\kappa/d\theta$. We note that at the reference state, $\alpha_0 = \alpha(\theta_0)$, $\kappa_0 = \kappa(\theta_0)$, $J_e = 1$, $p = 0$ and $\rho = \rho_0$. Thus, we recover the canonical relation between the heat capacities, where $\partial^2 U_e / \partial J_e^2 = \partial p / \partial J_e \rightarrow \kappa$ for typical volumetric potentials [25]. The novel Eqs. 16 and 18 provide continuum nonlinear descriptions of c_p and c_v for general thermo-mechanical systems.

The model is implemented into a two-dimensional finite element solver using a staggered isothermal split [28, 29]. For the mechanical problem, we implement generalized plane strain conditions [30] wherein we select the motion in the third direction such that $\sigma_{33} \approx (\sigma_{11} + \sigma_{22})/2$, emulating an isotropic stress response. The model is calibrated from experimental data and calibrated parameters are within the ranges of values reported in the literature.

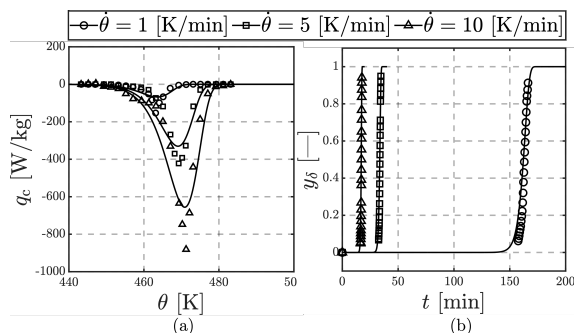


FIG. 1: Calibration of the chemical model. (a) The chemical heating as a function of temperature, used to calibrate the enthalpy of reaction, Δh^{rxn} , and the corrective factor, \hat{A} . (b) The mass fraction as a function of time. In each graph, the curves are plots of the model while the markers indicate experimental data from [19].

For the chemical model, Weese et al. [19] measured the kinetics of the HMX $\beta \rightarrow \delta$ phase transformation for heating rates of 1, 2, 5, and 10 [K/min]. They determined first order reaction parameters $A = 2.000 \times 10^{48}$ [s $^{-1}$] and $E_a = 432.0$ [kJ/mol]. By substituting Eq. 9 into Eq. 5 and simplifying, we find the evolution equation for the δ -HMX mass fraction

$$\dot{y}_\delta = k_c(1 - y_\delta). \quad (19)$$

Next, we perform a least squares fit using Eq. 19 and

Eq. 17a to the DSC heat release data for each heating rate. The corrective factor, \hat{A} , is assumed to vary linearly as a function of temperature rate and is calibrated as

$$\hat{A}(\dot{\theta}) = 0.0451\dot{\theta} + 0.0088. \quad (20)$$

This calibration also yields enthalpy of reaction, $\Delta h^{\text{rxn}} = 44.87$ [kJ/kg]. Figure 1(a) shows the results of the calibration for the 1, 5, and 10 [K/min] heating rates, while Figure 1(b) shows the associated y_δ curves.

For the CTE model, Weese and Burnham [16] performed measurements of the thermal dimensional change of HMX powders. This data corresponds to expansion with $\sim 17\%$ volume change because of the CTE as well as porosity. However, the volume change from β - to δ -HMX is 6.7% [16]. With this in mind, we propose a model to capture the overall thermal expansion as

$$\alpha(\theta) = \alpha_0 + \frac{\alpha_1 e^{-\omega(\theta - \theta_T)}}{[1 + e^{-\omega(\theta - \theta_T)}]^2}, \quad (21)$$

where α_0 , α_1 , ω , and θ_T are material parameters. The axial thermal strain can be computed from

$$\Delta L/L_0 = \int_{\theta_0}^{\theta} \alpha(\hat{\theta}) d\hat{\theta}, \quad (22)$$

where $L_0 = 3.54$ [mm] is the initial specimen length from [16]. We use the result of the integration in Eq. 22 to calibrate the CTE parameters in two stages. In the first stage, we utilize the data provided in [16] to calibrate the shape parameter, $\omega = 0.4794$ [K $^{-1}$], the transition temperature, $\theta_T = 465.8$ [K], and initial guesses for α_0 and α_1 . In the second stage, we calibrate α_0 and α_1 such that the total volume change, $\vartheta^3 - 1$, approximately matches the value of 6.7%. This yields $\alpha_0 = 2.443 \times 10^{-5}$ [K $^{-1}$] and $\alpha_1 = 0.007$ [K $^{-1}$]. Figure 2 shows the results of the calibration.

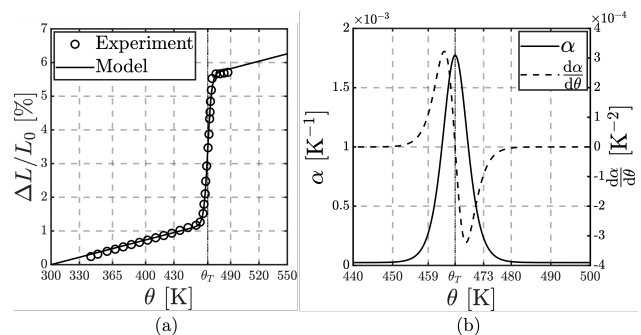


FIG. 2: Calibration of the CTE model. (a) Thermal strain of HMX powders as a function of temperature to calibrate the shape parameter, ω , and CTE transition temperature, θ_T . (b) The resulting nonlinear CTE and its derivative. The vertical lines on each plot mark θ_T .

For the thermo-mechanical model, Dobratz and Crawford [31] provide data to calibrate the thermal conductivity as $\Lambda = 0.5560$ [W/(m·K)], reference heat capacities as ${}^0c_p = 1035$ [J/(kg·K)] and ${}^0c_v = 1026$ [J/(kg·K)], and reference density as $\rho_0 = 1910$ [kg/m³]. Very little is known about the behavior of the bulk modulus for HMX during the phase transition. However, phase transition experiments on quartz [8] and on polymer gels [9] have shown precipitous decrease of the bulk modulus close to the phase transition temperature. For HMX, Levitas et al. [32] proposed that the $\beta \rightarrow \delta$ transition occurs via the stress-induced virtual melting mechanism. Therefore, we postulate that the bulk modulus will also substantially decrease and propose a nonlinear model given as

$$\kappa(\theta) = f_\kappa(\kappa_0 + \kappa'_0(\theta - \theta_0)) + (1 - f_\kappa)\kappa_1, \quad (23)$$

$$f_\kappa(\theta) \equiv \frac{1}{2} \left[1 - \tanh\left(\frac{\xi_0}{2}\right) \right] + \frac{1}{2} \left[1 + \tanh\left(\frac{\xi_1}{2}\right) \right],$$

where $\xi_0 = \theta - \theta_T - \phi_0$ and $\xi_1 = \theta - \theta_T - \phi_1$. Selection of the material parameters $\kappa_0 = 11000$ [MPa], $\kappa'_0 = -8.0$ [MPa/K], $\kappa_1 = 2000$ [MPa], $\phi_0 = -10.8$ [K], and $\phi_1 = 9.2$ [K] are guided using molecular dynamics simulations from Long and Chen [33] and Cui et al. [34]. Finally, we assume a constant Poisson ratio of $\nu = 0.31$ [-] [31], and the shear modulus is computed using the canonical relation $\mu(\theta) = 3\kappa(\theta)(1 - 2\nu)/(2(1 + \nu))$. Figure 3 shows the calibration results for $\kappa(\theta)$ and $\kappa'(\theta)$.

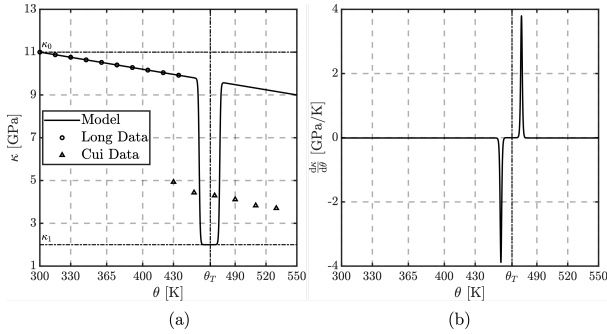


FIG. 3: Calibration of the bulk modulus model. (a) Bulk modulus of HMX as a function of temperature. (b) Derivative of the bulk modulus as a function of temperature. The vertical lines on each plot mark θ_T .

For the numerical simulations, a 1 mm \times 1 mm crystal of HMX is heated at the boundary, Γ , at a steady rate, $\dot{\theta}_\Gamma$, from an initial temperature of $\theta_0 = 300$ [K]. We consider temperature rates of 1, 5, and 10 [K/min] and simulation times of 15000, 3000, and 1500 [s] to achieve a final temperature of 550 [K]. To provide well resolved results, we have performed a mesh verification and used an adaptive time stepping strategy as in [28, 29].

Figure 4(a) shows the specific heats at constant elas-

tic strains, c_p , and volume, c_v , averaged over the computational cell. We observe large changes in magnitude for both specific heats (i.e., c_p will increase to ≈ 14840 [J/(kg·K)] and c_v will decrease to ≈ 528 [J/(kg·K)]). In light of Eqs. 16 and 18, the model predicts that the highly nonlinear $\alpha(\theta)$, $\kappa(\theta)$, and their derivatives (see Figure 2(b) and Figure 3) play a large role and compete in a highly nonlinear fashion. We note that our model predicts $\approx 6.7\%$ average volume change computed as $\Delta V/V_0 = J - 1$, which compares favorably to the theoretical estimate [16]. Furthermore, we observe a rapid temperature rate decrease and subsequent increase due to the nonlinearity of specific heats (see Figure 4(b)). However, the overall temperature rate variations with respect to the boundary heating rate, $\dot{\theta}_\Gamma$, are small in part due to the crystal size.

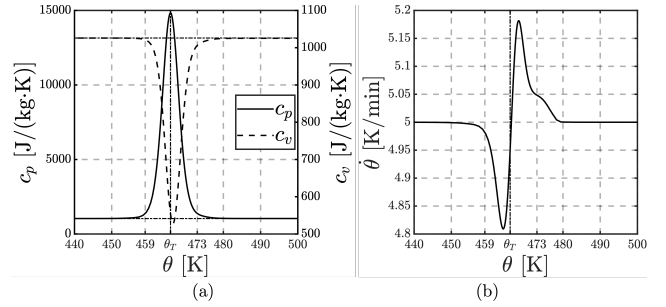


FIG. 4: (a) Specific heats at constant pressure and volume as functions of temperature. Horizontal dotted lines indicate the respective reference quantities 0c_p and 0c_v . (b) The temperature rate as a function of average cell temperature. Both results are from the simulation with 5 [K/min] boundary temperature rate.

This is a surprising result not observed for HMX that requires a careful analysis. First, we note that experimental results on specific heat of HMX often consider individual phases separately [35, 36]. Moreover, measurements are often performed at relatively large temperature intervals potentially under-resolving the transition that occurs over a narrow temperature range. Furthermore, spikes in DSC traces for HMX have been observed [35]. Levitas et al. [32] estimated that the elastic energy relaxed during the stress-induced virtual melting is $\Delta h \sim 30649$ [J/kg]. Considering the transition window of $\Delta\theta \sim 5.358$ [K] as shown in Figure 4(a) (i.e., computed as an average transition temperature interval over the c_p profile), we estimate change of the specific heat during the stress-induced virtual melting as $\Delta c_p = \Delta h / \Delta\theta \sim 5720.2$ [J/(kg·K)]. This value is smaller than our predictions, but we point to large material data sensitivity of $\alpha(\theta)$ and $\kappa(\theta)$. Second, we note that nonlinear CTEs are common in phase transitioning materials [12–14, 37] and that the c_p profile in Figure 4(a) is similar to DSC measurements on geopolymers concrete [7]. Therefore, the nonlinearity of c_p as predicted

by our model is plausible.

Finally, we note some model limitations. Specifically, the Helmholtz free energy, especially its thermal part in Eq. 10, is not well known. Moreover, we note the lack of pressure dependency and reaction reversibility [15], as well as crystal anisotropy, and pressure and temperature dependency of elastic parameters, especially κ [38].

We continue by deriving a novel estimate for the critical temperature at which the chemical heating rate occurs. Substituting the y_δ approximation, Eq. 19, into the chemical heating rate, Eq. 17a, setting the derivative of the resulting q_c with respect to θ equal to 0, then solving for θ , we find

$$\theta_c(\dot{\theta}) \approx \frac{E_a/R_u}{2W\left(\sqrt{\left(\frac{A\hat{A}E_a}{4\dot{\theta}R_u}\right)}\right)}, \quad (24)$$

where W is the W Lambert function [39]. For our parameters, θ_c tends to 474.2 [K] as $\dot{\theta}$ tends to infinity. In Figure 5(a), we plot the chemical heating rate averaged over the computational cell for each boundary temperature rate. For each $\dot{\theta}_\Gamma$, we note the associated critical temperature, θ_c , at which the chemical heating rate extremum occurs. We mark these $(\dot{\theta}_\Gamma, \theta_c)$ coordinate pairs in Figure 5(a). In Figure 5(b), we plot the $(\dot{\theta}_\Gamma, \theta_c)$ coordinate pairs alongside the predictions from Eq. 24. We note the remarkable agreement between the critical temperatures from simulations and those predicted by this equation. Furthermore, this provides a solution verification of the computational results.

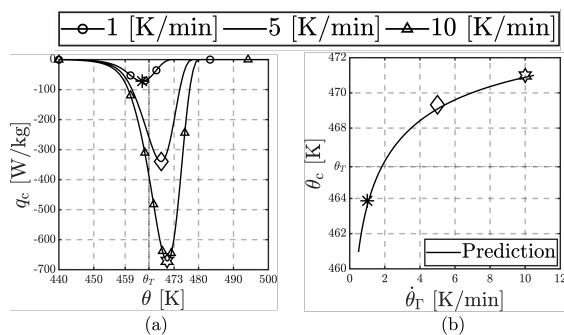


FIG. 5: (a) Chemical heating rate as a function of temperature and (b) critical temperature for the chemical heating rate as a function of boundary heating rate.

In conclusion, a thermodynamically consistent continuum chemo-thermo-mechanical model which provides general nonlinear equations for the specific heat at constant elastic strains and volume is derived. The model is implemented into a numerical solver and applied to the HMX $\beta \rightarrow \delta$ phase transition using parameters calibrated with experimental data. Simulation results predict highly non-

linear, exotic specific heat behavior including large spikes in magnitude. A novel estimate for the critical temperature at which the chemical heating rate extremum occurs is also derived.

This work was supported by the Department of Energy, National Nuclear Security Administration, under the reward No. DE-NA0002377 as part of the Predictive Science Academic Alliance Program II. We would also like to acknowledge support from Los Alamos National Laboratory under award No. 625808.

* Electronic address: kmatous@nd.edu

- [1] P. Lamberg, R. Lehtiniemi, and A.-M. Henell, *International Journal of Thermal Sciences* **43**, 277 (2004), ISSN 1290-0729, URL <https://www.sciencedirect.com/science/article/pii/S1290072903001303>.
- [2] V. D. Cao, S. Pilehvar, C. Salas-Bringas, A. M. Szczotok, T. Q. Bui, M. Carmona, J. F. Rodriguez, and A.-L. Kjøniksen, *Energy and Buildings* **173**, 678 (2018), ISSN 0378-7788, URL <https://www.sciencedirect.com/science/article/pii/S0378778817339245>.
- [3] S. Enibe, *Renewable Energy* **28**, 2269 (2003), ISSN 0960-1481, URL <https://www.sciencedirect.com/science/article/pii/S0960148103000715>.
- [4] F. Tan, S. Hosseinizadeh, J. Khodadadi, and L. Fan, *International Journal of Heat and Mass Transfer* **52**, 3464 (2009), ISSN 0017-9310, URL <https://www.sciencedirect.com/science/article/pii/S0017931009001896>.
- [5] D. Lynden-Bell and R. Lynden-Bell, *Monthly Notices of the Royal Astronomical Society* **181**, 405 (1977).
- [6] T.-C. Ling (Bill) and C. S. Poon, *Construction and Building Materials* **46**, 55 (2013).
- [7] V. D. Cao, T. Bui, and A.-L. Kjøniksen, *Energy* **186** (2019).
- [8] R. J. Angel, M. Alvaro, R. Miletich, and F. Nestola, *Contributions to Mineralogy and Petrology* **172**, 29 (2017), URL <https://doi.org/10.1007/s00410-017-1349-x>.
- [9] S. Hirotsu, *The Journal of Chemical Physics* **94**, 3949 (1991), <https://doi.org/10.1063/1.460672>, URL <https://doi.org/10.1063/1.460672>.
- [10] L. Landau and E. Lifshits, *Statistical Physics*, A-W series in advanced physics (Addison-Wesley Publishing Company, 1969), ISBN 9780201041675, URL https://books.google.com/books?id=_ZceAQAIAAJ.
- [11] A. Tröster, W. Schranz, F. Karsai, and P. Blaha, *Phys. Rev. X* **4**, 031010 (2014), URL <https://link.aps.org/doi/10.1103/PhysRevX.4.031010>.
- [12] J. B. Baldo and W. N. d. Santos, *Cerâmica* **48**, 172 (2002), ISSN 0366-6913, URL http://www.scielo.br/scielo.php?script=sci_arttext&pid=S0366-69132002000300011&nrm=iso.
- [13] S. M. Selbach, J. R. Tolchard, A. Fossdal, and T. Grande, *Journal of Solid State Chemistry* **196**, 249 (2012), ISSN 0022-4596, URL <https://www.sciencedirect.com/science/>

- article/pii/S0022459612003982.
- [14] S. Ran, C. T. Wolowicz, I. Jeon, N. Pouse, N. Kanchanavatee, B. D. White, K. Huang, D. Martien, T. DaPron, D. Snow, et al., *Proceedings of the National Academy of Sciences* **113**, 13348 (2016), ISSN 0027-8424, <https://www.pnas.org/content/113/47/13348.full.pdf>, URL <https://www.pnas.org/content/113/47/13348>.
- [15] R. Karpowicz and T. Brill, *AIAA Journal* **20**, 1586 (1982).
- [16] R. Weese and A. Burnham, *Propellants, Explosives, Pyrotechnics* **30**, 344 (2005).
- [17] B. F. Henson, L. Smilowitz, B. W. Asay, and P. M. Dickson, *J. Chem. Phys.* **117**, 3780 (2002).
- [18] L. Smilowitz, B. F. Henson, B. W. Asay, and P. M. Dickson, *J. Chem. Phys.* **117**, 3789 (2002).
- [19] R. Weese, J. Maienschein, and C. Perrino, *Thermochimica Acta* **401**, 1 (2003).
- [20] A. P. Wemhoff, A. K. Burnham, and A. L. Nichols, *The Journal of Physical Chemistry A* **111**, 1575 (2007), URL <https://doi.org/10.1021/jp066168+>.
- [21] E. Lee, *Journal of Applied Mechanics* **36**, 1 (1969).
- [22] J. M. Powers, *Combustion Thermodynamics and Dynamics* (Cambridge University Press, 2016).
- [23] L. Vujošević and V. Lubarda, *Theoretical and Applied Mechanics* **28–29**, 379 (2002).
- [24] J. Simo and T. Hughes, *Computational Inelasticity* (Springer, 1998).
- [25] S. Doll and K. Schweizerhof, *Journal of Applied Mechanics* **67**, 17 (1999), ISSN 0021-8936, URL <https://doi.org/10.1115/1.321146>.
- [26] C. Truesdell and W. Noll, *The Non-Linear Field Theories of Mechanics* (Springer, 2004).
- [27] B. D. Coleman and W. Noll, *Archive for Rational Mechanics and Analysis* **13**, 167 (1963), URL <https://doi.org/10.1007/BF01262690>.
- [28] K. Srinivasan, K. Matouš, P. Geubelle, and T. Jackson, *J. Comput. Physics* **228**, 7883 (2009).
- [29] M. Shabouei, W. Subber, C. W. Williams, K. Matouš, and J. M. Powers, *Combustion and Flame* **207**, 153 (2019), ISSN 0010-2180, URL <http://www.sciencedirect.com/science/article/pii/S0010218019302512>.
- [30] A. Saada, *Elasticity Theory and Applications*, Pergamon unified engineering series (R.E. Krieger Publishing Company, 1983), ISBN 9780898745597, URL <https://books.google.com/books?id=IIUrAAAACAAJ>.
- [31] B. M. Dobratz and P. C. Crawford, UCRL-52997 (1985).
- [32] V. I. Levitas, B. F. Henson, L. B. Smilowitz, and B. W. Asay, *Phys. Rev. Lett.* **92**, 235702 (2004), URL <https://link.aps.org/doi/10.1103/PhysRevLett.92.235702>.
- [33] Y. Long and J. Chen, *Journal of Applied Physics* **118**, 115901 (2015), <https://doi.org/10.1063/1.4930812>, URL <https://doi.org/10.1063/1.4930812>.
- [34] H.-L. Cui, G.-F. Ji, X.-R. Chen, Q.-M. Zhang, D.-Q. Wei, and F. Zhao, *Journal of Chemical & Engineering Data* **55**, 3121 (2010), <https://doi.org/10.1021/je100009m>, URL <https://doi.org/10.1021/je100009m>.
- [35] L. G. Koshigoe, R. L. Shoemaker, and R. E. Taylor, *AIAA Journal* **22**, 1600 (1984), <https://doi.org/10.2514/3.8823>, URL <https://doi.org/10.2514/3.8823>.
- [36] D. M. Hanson-Parr and T. P. Parr, *Journal of Energetic Materials* **17**, 1 (1999), <https://doi.org/10.1080/07370659908216094>, URL <https://doi.org/10.1080/07370659908216094>.
- [37] D. I. Bolef and J. de Klerk, *Phys. Rev.* **129**, 1063 (1963), URL <https://link.aps.org/doi/10.1103/PhysRev.129.1063>.
- [38] T. D. Sewell, R. Menikoff, D. Bedrov, and G. D. Smith, *The Journal of Chemical Physics* **119**, 7417 (2003), <https://doi.org/10.1063/1.1599273>, URL <https://doi.org/10.1063/1.1599273>.
- [39] J. H. Lambert, *Acta Helvetica Physico-Mathematico-Anatomico-Botanico-Medica* **3**, 128 (1758).